Auger spectra following inner-shell ionization of Argon by a Free-Electron Laser

A. O. G. Wallis,[1] L. Lodi,[1] and A. Emmanouilidou[1]

[1] *Department of Physics and Astronomy, University College London, Gower Street, London WC1E 6BT, United Kingdom*

(Dated: May 16, 2014)

We explore the possibility of retrieving Auger spectra with FEL radiation. Using a laser pulse of 260 eV photon energy, we study the interplay of photo-ionization and Auger processes following the initial formation of a 2p inner-shell hole in Ar. Accounting for the fine structure of the ion states we demonstrate how to retrieve the Auger spectrum of $Ar^+ \rightarrow Ar^{2+}$. Moreover, considering two electrons in coincidence we also demonstrate how to retrieve the Auger spectrum of $Ar^{2+} \rightarrow Ar^{3+}$.

PACS numbers: 32.80.Fb, 41.60.Cr, 42.50.Hz, 32.80.Rm

arXiv:1405.3799v1 [physics.atom-ph] 15 May 2014

I. INTRODUCTION

The response of atoms to intense extreme ultraviolet (XUV) and X-ray Free-Electron-Lasers (FEL) is a fundamental theory problem. In addition, understanding FEL-driven processes is of interest for accurate modeling of laboratory and astrophysical plasmas. The fast progress in generating intense FEL pulses of femtosecond duration renders timely the study of FEL driven processes in atoms. Such processes include the formation of inner-shell vacancies by photo-absorption and the subsequent Auger decays. Exploring the interplay of photo-ionization and Auger processes is a key to understanding the rich electron dynamics underlying the formation of highly charged ions [1–3] and hollow atoms [2, 4, 5].

Auger spectra have attracted a lot of interest over the years with early studies involving the formation of an inner-shell hole following the impact of a particle, such as an electron [6–10]. From the early 80s, synchrotron radiation has largely replaced particle impact as a triggering mechanism of Auger processes [11–14]. Such studies include the detailed Auger spectrum following the decay of $Ar^+(2p^{-1})$ [15, 16]. The reason for using synchrotron radiation is that it is monochromatic and allows for well defined initial excitations in the soft and hard X-ray regime. A recent study with synchrotron radiation [17] involves the measurement of Auger spectra following the decay of the $Ar^{2+}(2p^{-1}v^{-1})$ ionic states; v^{-1} is a hole in a valence orbital and $Ar^{2+}(2p^{-1}v^{-1})$ is formed by single-photon double ionization.

In this work, we explore the feasibility of obtaining detailed Auger spectra using FEL radiation. FEL radiation allows for well-defined initial excitations. It also allows for the creation of multiple inner-shell holes resulting in multiple Auger decays; generally the Auger spectra thus generated have larger yields than those generated from synchrotron radiation. The increasing availability of FEL sources provides an additional motivation for the current study. We explore the interplay of photo-ionization and Auger processes in Ar interacting with a 260 eV FEL pulse, a photon energy sufficient to ionize a single inner-shell 2p electron in Ar. We compute the ion yields due to Auger and photo-ionization processes and study the ion yields dependence on the FEL pulse parameters. To do so we solve a set of rate equations [18, 19]. Initially, in the rate equations we only account for the electronic configuration of the ion states. This simplification allows us to gain insight into the processes involved and explore the optimal parameters for observing Auger spectra. We next proceed to fully account for the fine structure of the ion states in the rate equations. We subsequently obtain the detailed Auger spectrum of $Ar^+ \rightarrow Ar^{2+}$. Moreover, we demonstrate how the detailed Auger spectrum of $Ar^{2+} \rightarrow Ar^{3+}$ can be observed in an FEL two-electron coincidence experiment.

II. AUGER AND ION YIELDS EXCLUDING FINE STRUCTURE

We model the response of Ar to a 260 eV FEL pulse by formulating and solving a set of rate equations for the time dependent populations of the ion states [18, 19]. Our first goal is to gain insight into how the ion and Auger yields depend on the duration and intensity of the laser pulse. To do so, in this section, we simplify the theoretical treatment by accounting only for the electronic configuration, i.e, $(1s^a, 2s^b, 2p^c, 3s^d, 3p^e)$ of the ion states and not the fine structure of these states. By fine structure we refer to all possible $^{2S+1}L_J$ states for a given electronic configuration, accounting for spin-orbit coupling. To compute the Auger transition rates between different electron configurations we use the formalism introduced by Bhalla *et al.* [20] and refer to these transition rates as Auger group rates in accord with [20].

A. Rate equations

In the rate equations we account for single-photon ionization and Auger transitions. For the ion states considered the X-ray fluorescence widths are typically three orders of magnitude smaller than the Auger decay widths [21]; we can thus safely neglect the former. In Fig. 1, accounting for states up to Ar^{4+}, we illustrate the photo-ionization and Auger transitions between states with dif-

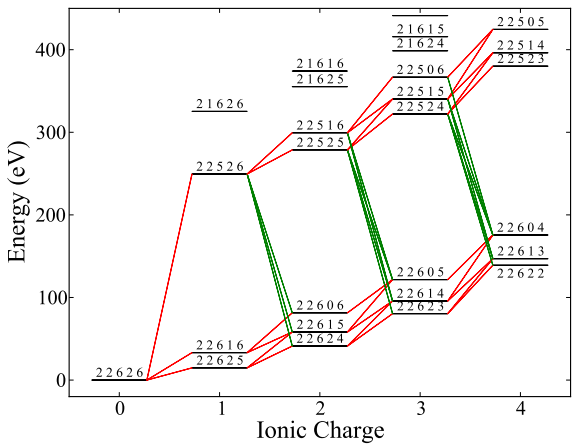

FIG. 1. (Color online) Ionization pathways between different electronic configurations of Ar, up to Ar^{4+}, accessible with sequential single-photon ($\hbar\omega = 260$eV) absorptions and Auger decays. The label (a, b, c, d, e) stands for the electronic configuration ($1s^a, 2s^b, 2p^c, 3s^d, 3p^e$). The red and green lines indicate photo-ionization and Auger transitions, respectively.

ferent electron configurations that are allowed for a laser pulse of 260 eV photon energy. This photon energy is sufficient for creating a single inner-shell 2p hole and multiple valence holes in Ar. In the rate equations we include all possible ion states accessible by a 260 eV laser-pulse; the highest ion state is $Ar^{9+}(1s^2, 2s^2, 2p^5, 3s^0, 3p^0)$. The rate equations describing the population $\mathcal{I}_i^{(q)}$ of an ion state i with charge q take the form

$$\begin{aligned}\frac{d}{dt}\mathcal{I}_j^{(q)}(t) &= \sum_i \left(\sigma_{i\to j}J(t) + \Gamma_{i\to j}\right)\mathcal{I}_i^{(q-1)}(t) \\ &\quad - \sum_k \left(\sigma_{j\to k}J(t) + \Gamma_{j\to k}\right)\mathcal{I}_j^{(q)}(t) \\ \frac{d}{dt}\mathcal{A}_{i\to j}^{(q)} &= \Gamma_{i\to j}\mathcal{I}_i^{(q-1)}(t), \\ \frac{d}{dt}\mathcal{P}_{i\to j}^{(q)} &= \sigma_{i\to j}J(t)\mathcal{I}_i^{(q-1)}(t),\end{aligned} \tag{1}$$

where $\sigma_{\mathrm{i}\to\mathrm{j}}$ and $\Gamma_{\mathrm{i}\to\mathrm{j}}$ are the single-photon absorption cross section and Auger decay rate from initial state i to final state j, respectively. J(t) is the photon flux. Atomic units are used in this work. The temporal form of the FEL flux is modelled with a Gaussian function [18] which is given by

$$J(t) = 1.554\times10^{-16}\frac{I_0[\mathrm{W\ cm^{-2}}]}{\hbar\omega[\mathrm{eV}]}\exp\left\{-4\ln 2\left(\frac{t}{\tau_X}\right)^2\right\} \tag{2}$$

with τ_X the full width at half maximum and I_0 the peak intensity. The first term in Eq. (1) accounts for the formation of the state j with charge q through the single-photon ionization and Auger decay of the state i with charge $q-1$. The second term in Eq. (1) accounts for the depletion of state j by single-photon ionization and Auger decay to the state k with charge $q+1$. In Eq. (1), we also solve for the Auger yield $\mathcal{A}_{i\to j}^{(q)}$ from an initial state i with charge $q-1$ to a final state j with charge q. In addition, we solve for the photo-ionization yield $\mathcal{P}_{i\to j}^{(q)}$ from an initial state i with charge $q-1$ to a final state j with charge q. These yields provide the probability for observing an electron with energy corresponding to the transition $\mathrm{i}\to\mathrm{j}$. The total Auger and photo-ionization yields for the transition from any state with charge $q-1$ to any state with charge q are given by

$$\mathcal{A}^{(q)} = \sum_{i,j}\mathcal{A}_{i\to j}^{(q)}, \qquad \mathcal{P}^{(q)} = \sum_{i,j}\mathcal{P}_{i\to j}^{(q)}. \tag{3}$$

To find the total ion yield of a state with charge q, i.e., the ion yield for Ar^{q+} we sum over the populations of all ion states with charge q

$$\mathcal{I}^{(q)} = \sum_i \mathcal{I}_i^{(q)}. \tag{4}$$

All yields are computed long after the end of the pulse.

As we show later in the paper, it is also of interest to compute the Auger and photo-ionization yields along a pathway $\mathrm{i}\to\mathrm{j}\to\mathrm{k}$. These yields provide the probability for observing in a two-electron coincidence experiment two electrons with energies corresponding to the transitions $\mathrm{i}\to\mathrm{j}$ and $\mathrm{j}\to\mathrm{k}$. If there is only one state i leading to state j then the probability for observing the electron emitted in the transition $\mathrm{i}\to\mathrm{j}$ and the electron emitted in the transition $\mathrm{j}\to\mathrm{k}$ is simply the Auger $\mathcal{A}_{j\to k}^{(q)}$ or the photo-ionization $\mathcal{P}_{j\to k}^{(q)}$ yield. However, it can be the case that we have multiple states leading to state j, for example, $\mathrm{i}\to\mathrm{j}\to\mathrm{k}$ and $\mathrm{i}'\to\mathrm{j}\to\mathrm{k}$. Then to compute the probability $\mathcal{P}_{j(i)\to k}^{(q)}$ or $\mathcal{A}_{j(i)\to k}^{(q)}$ for observing the electron emitted in the transition $\mathrm{i}\to\mathrm{j}$ and the electron emitted in the transition $\mathrm{j}\to\mathrm{k}$ we need to solve separately for the contribution of state i to the population of state j:

$$\begin{aligned}\frac{d}{dt}\mathcal{I}_{j(i)}^{(q-1)}(t) =& \left(\sigma_{i\to j}J(t) + \Gamma_{i\to j}\right)\mathcal{I}_i^{(q-2)}(t) \\ &- \sum_{k'}\left(\sigma_{j\to k'}J(t) + \Gamma_{j\to k'}\right)\mathcal{I}_{j(i)}^{(q-1)}(t) \\ \frac{d}{dt}\mathcal{P}_{j(i)\to k}^{(q)} =& \sigma_{j\to k}J(t)\mathcal{I}_{j(i)}^{(q-1)}(t) \\ \frac{d}{dt}\mathcal{A}_{j(i)\to k}^{(q)} =& \Gamma_{j\to k}\mathcal{I}_{j(i)}^{(q-1)}(t).\end{aligned} \tag{5}$$

B. Auger group rates

To compute the Auger group rates $\Gamma_{i\to j}$ we use the formulation of Bhalla et al. [20]. For each electron configuration included in the rate equations, we obtain the energy and bound atomic orbital with a Hartree-Fock (HF) calculation. These calculations are performed with

TABLE I. Auger group rates for a transition from an initial state ($1s^a, 2s^b, 2p^c, 3s^c, 3p^e$) to a final state where the electron filling in the 2p hole in the initial state and the electron escaping to the continuum occupy nl and n′l′ orbitals. We also list the Auger rates obtained in [28] using the Hartree-Fock-Slater (HFS) method, in [29] using a Hartree-Fock (HF) method, and in [29] using a CI calculation. The rates are given in 10^{-4} a.u.

initial config.					method	group rates (10^{-4} a.u.)			
a	b	c	d	e		$3s3s$	$3s3p$	$3p3p$	total
2	2	5	2	6	HFS [28]	0.77	12.85	47.90	61.52
					HF [29]	0.28	15.74	56.97	72.99
					CI [29]	0.47	9.54	54.74	64.75
					this work	0.45	15.60	51.67	67.72

the *ab initio* quantum chemistry package MOLPRO [22] using the split-valence 6-311G basis set. To compute the continuum orbital that describes the outgoing Auger electron we use the Hartree-Fock-Slater (HFS) one-electron potential that is obtained using an updated version of the Herman Skillman atomic structure code [23, 24]. This one electron potential is expressed in terms of an effective nuclear charge $Z_{\rm HFS}(r)$. The resulting radial HFS equation is of the form

$$\left[-\frac{d^2}{dr^2}+\frac{l(l+1)}{r^2}-\frac{Z_{\rm HFS}(r)}{r}\right]P_{nl}(r)=EP_{nl}(r), \quad (6)$$

where the orbital wavefunction is given by $\psi_{\rm nlm}(\mathbf{r}) = {\rm r}^{-1}{\rm P}_{\rm nl}({\rm r}){\rm Y}_{\rm lm}(\hat{\rm r})$. We solve equation Eq. (6) for the continuum orbital ($E > 0$) using the modified Numerov method [25, 26]. We match the solution to the appropriate asymptotic boundary conditions for energy normalized continuum wave functions [27]. In Table I we list our results for the Auger group rates $Ar^+(2p^{-1}) \rightarrow Ar^{2+}(3s^{-1}3p^{-1})$, $Ar^+(2p^{-1}) \rightarrow Ar^{2+}(3s^{-2})$ and $Ar^+(2p^{-1}) \rightarrow Ar^{2+}(3p^{-2})$ and compare them with two other calculations that employ the HFS method [28] and the HF method [29] both for the bound and the continuum orbitals. As expected, our results lie between the results of these two calculations. For reference, we also list in Table I the results from a Configurational Interaction (CI) calculation [29]. In Table II we list our results for all the Auger group rates involved in the rate equations for Ar for a 260 eV FEL pulse.

C. Results for Auger and Ion yields

For the photo-ionization cross sections we use the Los Alamos National Laboratory atomic physics codes [30] that are based on the HF routines of R. D. Cowan [31]. Assuming that the initial state is the neutral Ar, we solved numerically [32] the set of first order differential

TABLE II. As in Table I for results obtained in this work for all Auger group rates included in the rate equations.

initial config.					group rates (10^{-4} a.u.)			
a	b	c	d	e	$3s3s$	$3s3p$	$3p3p$	total
2	2	5	2	6	0.450	15.598	51.665	67.713
2	2	5	2	5	0.502	9.615	25.457	35.575
2	2	5	1	6	-	9.244	58.693	67.937
2	2	5	2	4	0.568	9.429	20.324	30.321
2	2	5	1	5	-	5.780	29.273	35.053
2	2	5	0	6	-	-	68.708	68.708
2	2	5	2	3	0.638	7.973	11.680	20.291
2	2	5	1	4	-	5.631	23.952	29.583
2	2	5	0	5	-	-	33.761	33.761
2	2	5	2	2	0.710	5.845	4.349	10.905
2	2	5	1	3	-	4.650	13.337	17.986
2	2	5	0	4	-	-	23.946	23.946
2	2	5	2	1	0.778	2.843	-	3.621
2	2	5	1	2	-	3.374	4.909	8.283
2	2	5	0	3	-	-	14.309	14.309
2	2	5	2	0	0.863	-	-	0.863
2	2	5	1	1	-	1.612	-	1.612
2	2	5	0	2	-	-	5.168	5.168

rate equations in Eq. (1). In Fig. 2 we show our results for the total ion $\mathcal{I}^{(q)}$ and Auger $\mathcal{A}^{(q)}$ yields as a function of the pulse intensity for pulse durations of 5 fs and 50 fs. From Fig. 2 we observe that $\mathcal{A}^{(q)}$ can be very similar to $\mathcal{I}^{(q)}$ for $q \geq 2$ depending on the pulse intensity and duration. Indeed, the formation of Ar^{q+} occurs from a sequence of transitions where the final step involves either the single-photon ionization or the Auger decay of $Ar^{(q-1)+}$. For high pulse intensities, independent of the pulse duration, both final steps are likely and thus $\mathcal{A}^{(q)}$ is different than $\mathcal{I}^{(q)}$. For small pulse intensities, if the pulse is short then the formation of Ar^{q+} through the Auger decay of $Ar^{(q-1)+}$ is favored; if the pulse is long multi-photon absorption is highly likely making possible formation of Ar^{q+} also through single-photon ionization of $Ar^{(q-1)+}$. Thus, generally, for small pulse intensities, if the pulse is short $\mathcal{A}^{(q)} \approx \mathcal{I}^{(q)}$ while if the pulse is long $\mathcal{A}^{(q)} \neq \mathcal{I}^{(q)}$.

D. Truncation of the number of states included in the rate equations

Fig. 2 shows that appropriate tuning of the laser parameters can result in large Auger yields even for high ion states. Regarding Auger spectra this is an advantage of FEL radiation compared to synchrotron radiation. However, discerning the Auger spectra produced by the FEL pulse is a challenging task since many photo-ionization

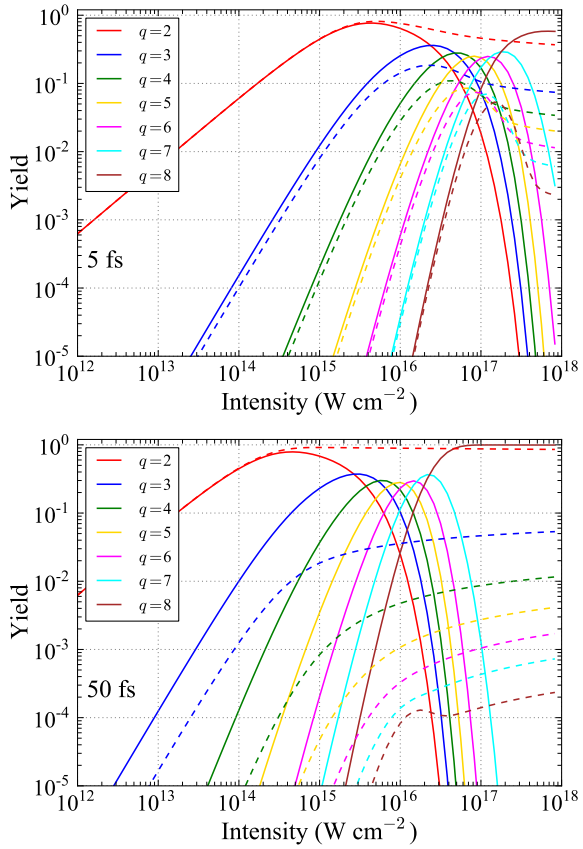

FIG. 2. (Color online) Total ion $\mathcal{I}^{(q)}$ (solid lines) and Auger $\mathcal{A}^{(q)}$ (dashed lines) yields as a function of intensity for pulse duration of 5 fs (top) and 50 fs (bottom).

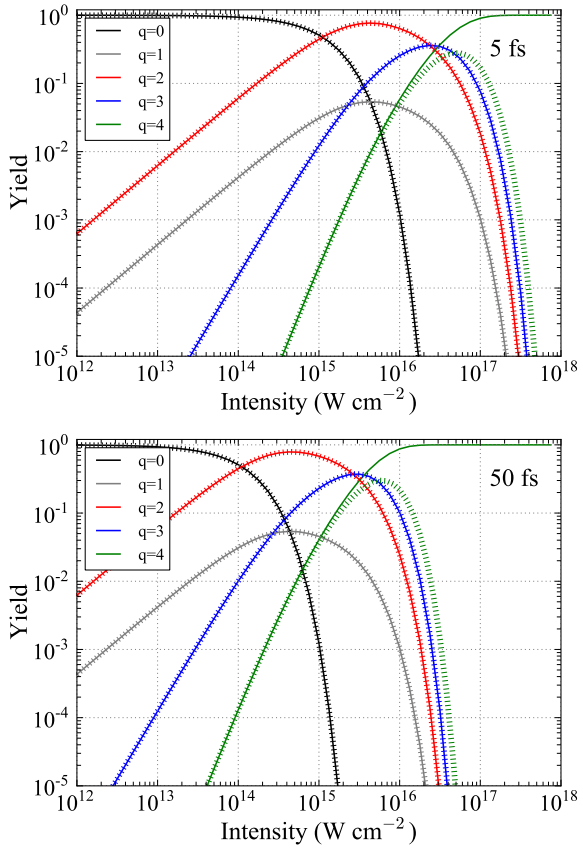

FIG. 3. (Color online) Total ion yields $\mathcal{I}^{(q)}$ for q = 0,1,2,3,4 when ion states up to Ar^{9+} (dashed lines) and ion states up to Ar^{4+} (solid lines) are included as a function of pulse intensity for pulse durations 5 fs (top) and 50 fs (bottom).

and Auger electrons escape to the continuum. In the next section we focus on the Auger electron spectra resulting from ion states up to Ar^{3+}. To accurately describe these spectra we need to account for the fine structure of the ion states included in the rate equations. However, such an inclusion results in a very large increase of the number of ion states that need to be accounted for in the rate equations. For instance, when considering states up to Ar^{4+} the number of ions states in the rate equations increases from 21(no fine structure) to 186 (with fine structure). We thus truncate the number of ion states we consider. In Fig. 3 we compare $\mathcal{I}^{(q)}$, for q = 1,2,3,4, when we include ion states up to Ar^{9+} and up to Ar^{4+}. We find that the truncation affects only $\mathcal{I}^{(4)}$ while $\mathcal{I}^{(1)}$, $\mathcal{I}^{(2)}$ and $\mathcal{I}^{(3)}$ are unaffected. Since the focus of the current work is the Auger electron spectra up to Ar^{3+}, in what follows we truncate to include only ion states up to Ar^{4+}. Moreover, comparing Fig. 3 with Fig. 2, we find that a pulse duration of 5 fs is short enough for $\mathcal{A}^{(q)} \approx \mathcal{I}^{(q)}$ to be true for intensities up to roughly 10^{16} W cm^{-2}. This guarantees that less photo-ionization electrons are ejected to the continuum making it easier to discern the Auger electrons. We also find that for pulse intensities around 10^{15}-10^{16} W cm^{-2} both $\mathcal{A}^{(2)}$ and $\mathcal{A}^{(3)}$ yields have significant values. Thus, a laser pulse with duration of 5 fs and intensity of 5×10^{15} W cm^{-2} is optimal for the experimental observation of the Auger electron spectra up to Ar^{3+}.

III. AUGER SPECTRA

A. Computation of fine structure ion states

We next describe the method we use to compute the fine structure states of each electron configuration that is included in the truncated rate equations. To obtain the fine structure ion states we use the GRASP2K package [33] and the RELCI extension [34] provided in the RATIP package [35]. These packages are used to perform relativistic calculations within the Multi-Configuration Dirac-Hartree-Fock (MCDHF) formalism [36]. The photo-ionization cross sections and Auger decay rates between fine structure states are then calculated using the PHOTO and AUGER components of the RATIP package. Since GRASP2K utilizes the Dirac equation the calculations are

performed in the j-j coupling scheme. We briefly outline the steps we follow to obtain the fine structure states for a given electron configuration of Ar; where appropriate we illustrate using $Ar^+(1s^2, 2s^2, 2p^5, 3s^2, 3p^6)$.

1) We identify the fine structure states for the electron configuration at hand; in our example these states are $^2P_{1/2}$ and $^2P_{3/2}$. We identify the configurational state functions (CSFs) that can be constructed out of the possible nlj orbitals; in our example the possible CSFs are

$$1.(1s^2_{1/2}, 2s^2_{1/2}, 2p^1_{1/2}, 2p^4_{3/2}, 3s^2_{1/2}, 3p^2_{1/2}, 3p^4_{3/2}); J^P = \frac{1}{2}^-$$

$$2.(1s^2_{1/2}, 2s^2_{1/2}, 2p^2_{1/2}, 2p^3_{3/2}, 3s^2_{1/2}, 3p^2_{1/2}, 3p^4_{3/2}); J^P = \frac{3}{2}^-$$

Each fine structure state is a linear combination of the CSFs that have the same total angular momentum J and parity P; in our example $^2P_{1/2}$ is expressed in terms of the first CSF and $^2P_{3/2}$ in terms of the second CSF. A Self-Consistent-Field (SCF) DHF calculation is now performed for all the CSFs. This calculation optimizes the nlj orbitals and the coefficients in the expansion of each fine structure state in terms of CSFs.

2) To account for electron correlation, as a first step, we include the additional orbitals $3d_{3/2}$ and $3d_{5/2}$. A new set of CSFs is generated from the single and double excitations of the step-1 CSFs, while keeping the occupation of the 1s, 2s and 2p orbitals frozen. A new MCDHF calculation is then performed with the new set of CSFs keeping the step-1 nlj orbitals frozen and only optimizing the newly added ones.

3) As a second step in accounting for electron correlation, we include all orbitals up to $4d_{3/2}$, $4d_{5/2}$. Again, as for step-2, a new set of CSFs is generated from the single and double excitations of the step-1 CSFs, while keeping the occupation of the $1s$, $2s$ and $2p$ orbitals frozen. Another MCDHF calculation is performed optimizing only the newly added, compared to step-2, orbitals. Introducing correlation orbitals layer by layer as described in steps 1-3 is the recommended procedure in the GRASP2K manual in order to achieve convergence of the SCF calculations.

4) Finally, using the orbitals generated in steps 1-3 we perform a CI calculation that optimizes the coefficients that express each fine structure state in terms of all the CSFs generated in steps 1-3.

In Table III we list the energies and Auger rates we obtain using the method described above for the fine structure states of $Ar^+(2p^{-1})$. To directly compare with the experimental results in [15] we define the intensity for an Auger decay from an initial state i to a final state j as

$$I_{i\to j} = \frac{\Gamma_{i\to j}}{\sum_j \Gamma_{i\to j}}, \tag{7}$$

and is scaled such that the intensity for the transition $Ar^+(2p^{-1}) \to Ar^{2+}(3p^{-2};^1S_0)$ is equal to 100 in accord with [15]. It can be seen that our calculated results are in good agreement with the experimental results of Pulkkinen *et al.* [15].

TABLE III. The Auger energies and rates from the $Ar(2p^{-1}_{1/2})$ and $Ar(2p^{-1}_{3/2})$ initial state to a final state where the electron filling in the 2p hole and the electron escaping to the continuum occupy nl and n′l′ orbitals. We list the MCDHF results obtained in this work and the experimental results of Pulkkinen *et al.* [15]. The Auger electron energies E are given in eV and the Auger rates Γ are given in 10^{-4} a.u.

Final State		Exp. [15]		this work		
		E	I	E	Γ	I
$Ar^+(2p^{-1}_{1/2})$						
$3p3p$	$^3P_2$	207.39	76	207.57	2.37	64
	$^3P_1$	207.25	176	207.44	5.11	138
	$^3P_0$	207.20	60	207.38	2.13	58
	$^1D_2$	205.65	404	205.64	11.78	318
	$^1S_0$	203.26	100	203.35	3.70	100
$3s3p$	$^3P_2$	-	-	193.25	0.02	1
	$^3P_1$	193.13	24	193.12	1.12	30
	$^3P_0$	193.07	18	193.06	0.58	16
	$^1P_1$	189.50	39	188.66	1.85	50
$3s3s$	$^1S_0$	176.43	6	175.36	0.62	17
$Ar^+(2p^{-1}_{3/2})$						
$3p3p$	$^3P_2$	205.24	261	205.43	7.58	240
	$^3P_1$	205.10	73	205.30	2.77	88
	$^3P_0$	205.08	26	205.24	0.73	23
	$^1D_2$	203.50	390	203.50	11.01	348
	$^1S_0$	201.11	100	201.22	3.16	100
$3s3p$	$^3P_2$	191.09	77	191.11	1.52	48
	$^3P_1$	190.95	11	190.98	0.35	11
	$^3P_0$	-	-	190.92	0	0
	$^1P_1$	187.39	71	186.52	1.79	57
$3s3s$	$^1S_0$	174.27	13	173.22	0.61	19

B. Results for Auger and Ion yields including fine structure

In Fig. 4 we show the total ion $\mathcal{I}^{(q)}$ and Auger $\mathcal{A}^{(q)}$ yields accounting for fine structure for a pulse duration of 5 fs. We find that these yields are very similar to the yields obtained in the previous section where fine structure was neglected. Thus our conclusions in the previous section regarding optimal laser parameters for observing the Auger electron spectra up to Ar^{3+} still hold. Also in Fig. 5 we plot the Auger yields $\mathcal{A}^{(2)}_{i\to j}$ and $\mathcal{A}^{(3)}_{i\to j}$ for all possible i, j fine structure states.

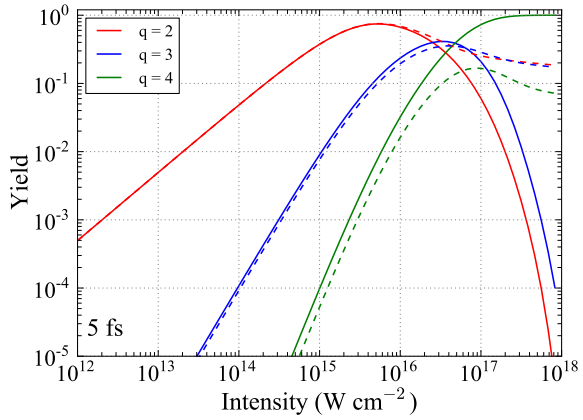

FIG. 4. (Color online) Total ion $\mathcal{I}^{(q)}$ (solid lines) and Auger $\mathcal{A}^{(q)}$ yields (dashed lines) for $q = 2, 3, 4$ as a function of intensity for a pulse duration of 5 fs. These yields are calculated with fine structure included in the rate equations.

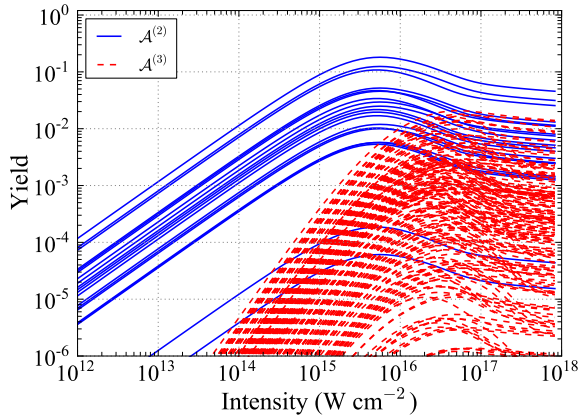

FIG. 5. (Color online) The Auger yields $\mathcal{A}^{(2)}_{i\to j}$ (blue, solid lines) and $\mathcal{A}^{(3)}_{i\to j}$ (red, dashed lines) as a function of intensity for a pulse duration of 5 fs. These yields are calculated with fine structure included in the rate equations.

C. Auger spectra including fine structure

1. *One-electron Auger spectra*

In Fig. 6 we compute the electron spectra for a 260 eV FEL pulse with 5×10^{15} W cm^{-2} intensity and 5 fs duration. Both the Auger $\mathcal{A}^{(q)}_{i\to j}$ and photo-ionization $\mathcal{P}^{(q)}_{i\to j}$ yields for charges up to $q = 4$ contribute to the peaks in these electron spectra. To account for the energy uncertainty of a 5 fs pulse, which is 0.37 eV, we have convoluted the peaks in Fig. 6 with Gaussian functions of 0.37 eV FWHM. We find that the energies of the photo-ionization electrons ejected in the transition $Ar^+ \to Ar^{2+}$ (peak height $\mathcal{P}^{(2)}_{i\to j}$) are well separated from the energies of the Auger electrons ejected in the transitions $Ar^+ \to Ar^{2+}$ (peak height $\mathcal{A}^{(2)}_{i\to j}$) and $Ar^{2+} \to Ar^{3+}$ (peak height $\mathcal{A}^{(3)}_{i\to j}$); the photo-ionization peaks are above 210 eV while the Auger peaks are below 210 eV. In Fig. 6 and Table IV, the energy range of the photo-ionization electrons is denoted by A, B, C; the energy range of the Auger electrons emitted during transitions from the initial states Ar^+ and Ar^{2+} are denoted by D, E, F, and E, F, and G, respectively. In Fig. 6 we see that the Auger yields $\mathcal{A}^{(2)}_{i\to j}$ (D, E, F) are much larger than all other Auger yields in the same energy range. They can thus

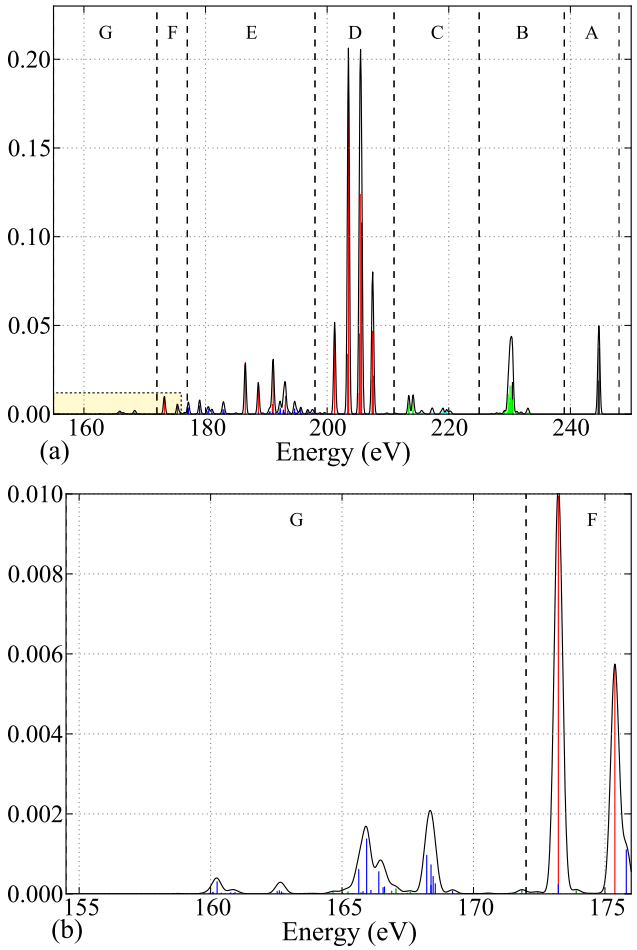

FIG. 6. (Color online) The electron spectra for a 5 fs, 260 eV pulse with an intensity of 5×10^{15} W cm^{-2} for energies between 150 and 250 eV (a) and energies between 155 and 177 eV (b). For clarity the plot range of (b) is highlighted in yellow in (a). The peaks are convoluted by 0.37 eV FWHM Gaussian functions. The peaks of the photo-ionization electrons emitted during transitions from the initial states Ar (black) and Ar^+ (green) are in the energy ranges denoted by A, B, and C (see Table IV). The peaks of the Auger electrons emitted during the transitions $Ar^+(2p^{-1}) \to Ar^{2+}$ (red) are in the energy ranges denoted by D, E, and F, and the ones emitted during the transitions $Ar^{2+}(2p^{-1}v^{-1}) \to Ar^{3+}$ (blue) are in the energy ranges denoted by E, F, and G (see Table IV).

TABLE IV. Labeling of energy regions in the electron spectrum shown in Fig. 6. $e_{\rm P}^-$ and $e_{\rm A}^-$ stand for photo-ionization and Auger electrons, respectively. u^{-1} represents a hole in any of the $2p$, $3s$ or $3p$ orbitals.

Region	Transitions
A	$\mathrm{Ar}+\hbar\omega \rightarrow \mathrm{Ar}^+(3p^{-1}) + e_{\rm P}^-$
B	$\mathrm{Ar}+\hbar\omega \rightarrow \mathrm{Ar}^+(3s^{-1}) + e_{\rm P}^-$
B	$\mathrm{Ar}^+(u^{-1}) + \hbar\omega \rightarrow \mathrm{Ar}^{2+}(u^{-1}3p^{-1}) + e_{\rm P}^-$
C	$\mathrm{Ar}^+(u^{-1}) + \hbar\omega \rightarrow \mathrm{Ar}^{2+}(u^{-1}3s^{-1}) + e_{\rm P}^-$
D	$\mathrm{Ar}^+(2p^{-1}) \rightarrow \mathrm{Ar}^{2+}(3p^{-2}) + e_{\rm A}^-$
E	$\mathrm{Ar}^+(2p^{-1}) \rightarrow \mathrm{Ar}^{2+}(3s^{-1}3p^{-1}) + e_{\rm A}^-$
F	$\mathrm{Ar}^+(2p^{-1}) \rightarrow \mathrm{Ar}^{2+}(3s^{-2}) + e_{A}^-$
E, F, G	$\mathrm{Ar}^{2+}(2p^{-1}v^{-1}) \rightarrow \mathrm{Ar}^{3+}(v^{-3}) + e_{A}^-$

be discerned and measured for the laser parameters under consideration. The Auger yields $\mathcal{A}^{(3)}_{i\rightarrow j}$ (E, F, G) are smaller but still visible, while the Auger yields $\mathcal{A}^{(4)}_{i\rightarrow j}$ are too small to be discerned in Fig. 6. However, except for the energy region below 170 eV, the Auger electron spectra resulting from the transitions $\mathrm{Ar}^{2+} \rightarrow \mathrm{Ar}^{3+}$ overlap with the Auger electron spectra resulting from the transitions $\mathrm{Ar}^{+} \rightarrow \mathrm{Ar}^{2+}$. Thus, in order to discern and be able to experimentally observe the latter Auger electron spectra we need to consider spectra of two electrons in coincidence. We do so in what follows.

2. *Two-electron coincidence Auger spectra*

We now consider the electron spectra resulting from the transitions:

$$\mathrm{Ar} + \hbar\omega \rightarrow \mathrm{Ar}^+(2p^{-1}) + e_P^- \rightarrow \mathrm{Ar}^{3+} + e_P^- + e_B^- + e_C^- \quad (8)$$

The photo-ionization electron $\mathrm{e}_{\rm P}^-$ has an energy of 12.3 eV for $\mathrm{Ar}^+(2p_{3/2}^{-1})$ and 10.2 eV for $\mathrm{Ar}^+(2p_{1/2}^{-1})$. This energy is very different from the energies of electrons $\mathrm{e}_{\rm B}^-$ and $\mathrm{e}_{\rm C}^-$. It thus suffices to plot in coincidence the energies of electrons $\mathrm{e}_{\rm B}^-$ and $\mathrm{e}_{\rm C}^-$. We note that many coincidence experiments have been performed with synchrotron radiation [12, 14, 16, 17]. While some coincidence experiments have been performed with FEL radiation [37, 38] the low repetition rate poses a challenge. Advances in FEL sources should overcome such challenges in the near future.

In Fig. 7 we plot in coincidence the energies of electrons $\mathrm{e}_{\rm B}^-$ and $\mathrm{e}_{\rm C}^-$. Specifically, Fig. 7 corresponds to the $\mathrm{Ar}^+(2p_{3/2}^{-1})$ fine structure state in Eq. (8). We only show the spectrum that lies below the line $E_B = E_C$ (black solid line), with E_B the energy of electron $\mathrm{e}_{\rm B}^-$ and E_C the energy of electron $\mathrm{e}_{\rm C}^-$. Since the two electrons are indistinguishable, the remaining spectrum can be obtained by a reflection with respect to the line $E_B = E_C$ of

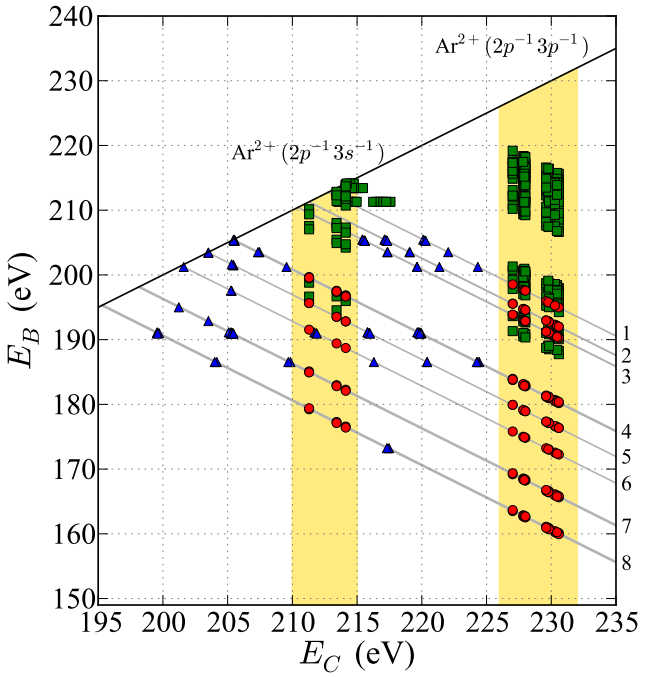

FIG. 7. (Color online) Two-electron coincidence spectra for $\mathrm{Ar}^+(2p_{3/2}^{-1}) \rightarrow \mathrm{Ar}^{3+}(v^{-3})$ generated by a 5 fs, 5×10^{15} W cm^{-2} FEL pulse. We show the spectrum below the $E_B = E_C$ line for the PPP (green squares), PAP (blue triangles) and PPA (red circles) transition sequences, see text for details. The $\mathrm{Ar}^{3+}(3p^{-3})$ final fine structure states are labeled as 1:^4S, 2:^2D, 3:^2P, the $\mathrm{Ar}^{3+}(3s^{-1}3p^{-2})$ states as 4:^4P, 5:^2D, 6:^2S, 7:^2P, and the $\mathrm{Ar}^{3+}(3s^{-2}3p^{-1})$ state as 8:^2P. The energy range of the PPA transition sequences $\mathrm{Ar}^+(2\mathrm{p}^{-1}) \rightarrow \mathrm{Ar}^{2+}(2\mathrm{p}^{-1}3\mathrm{s}^{-1}) \rightarrow \mathrm{Ar}^{3+}$ and $\mathrm{Ar}^+(2\mathrm{p}^{-1}) \rightarrow \mathrm{Ar}^{2+}(2\mathrm{p}^{-1}3\mathrm{p}^{-1}) \rightarrow \mathrm{Ar}^{3+}$ are highlighted by yellow.

the spectrum shown in Fig. 7. From Eq. (8) it follows that each line with $E_B + E_C = constant$, grey lines in Fig. 7, scans the spectra of electrons emitted from transitions in Eq. (8) through any possible fine structure state of Ar^{2+} to the same fine structure state of Ar^{3+}. The spectra of the electrons emitted from the transitions in Eq. (8) can be labelled according to the sequence of photo-ionization (P) and Auger processes (A) involved while transitioning from Ar to Ar^{3+}: PPA (red in Fig. 7), PPP (green) and PAP (blue). Our goal is to retrieve the Auger electron spectra corresponding to the transitions $\mathrm{Ar}^{2+} \rightarrow \mathrm{Ar}^{3+}$. These latter spectra are the ones labelled as PPA in Fig. 7; we highlight the energy range of the $\mathrm{e}_{\rm B}^-$ and $\mathrm{e}_{\rm C}^-$ electrons emitted in the PPA transition sequences $\mathrm{Ar}^+(2\mathrm{p}^{-1}) \rightarrow \mathrm{Ar}^{2+}(2\mathrm{p}^{-1}3\mathrm{s}^{-1}) \rightarrow \mathrm{Ar}^{3+}$ and $\mathrm{Ar}^+(2\mathrm{p}^{-1}) \rightarrow \mathrm{Ar}^{2+}(2\mathrm{p}^{-1}3\mathrm{p}^{-1}) \rightarrow \mathrm{Ar}^{3+}$. Thus to be able to retrieve the Auger electron spectra associated with the transitions $\mathrm{Ar}^{2+} \rightarrow \mathrm{Ar}^{3+}$ we must be able to discern the PPA from the PPP and the PAP transition sequences. We see that in the highlighted area in Fig. 7 there is some small overlap of the PPA with the

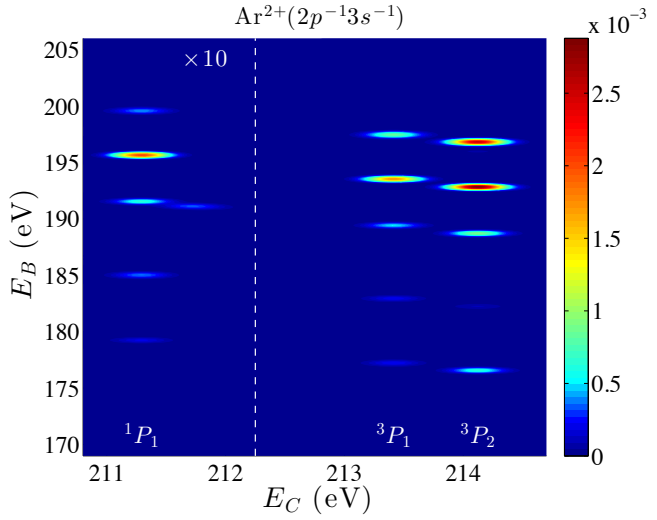

FIG. 8. (Color online) Two-electron coincidence spectra for $Ar^+(2p^{-1}) \rightarrow Ar^{2+}(2p^{-1}3s^{-1}) \rightarrow Ar^{3+}$ for the $Ar^{2+}(2p^{-1}3s^{-1})$ fine structure states $^1P_1$, $^3P_1$ and $^3P_2$. The peaks of the spectra corresponding to the $Ar^{2+}(2p^{-1}3s^{-1};^1P_1)$ fine structure state, to the left of the vertical dashed-white line, are much smaller than the rest of the spectra and we have thus multiplied them by a factor of 10 so that they are visible. The coincidence peaks have been convoluted by 0.37 eV FWHM Gaussian functions.

PPP and PAP sequences. However, we find that the height of the peaks of the PPA transition sequences are much larger than the height of the peaks of the PPP and PAP transition sequences. Specifically, the total Auger yield $\mathcal{A}^{(3)}$ associated with the PPA transition sequences is roughly 5 times larger than the photo-ionization yield $\mathcal{P}^{(3)}_{PAP}$ corresponding to the PAP transition sequences and 10 times larger than the photo-ionization yield $\mathcal{P}^{(3)}_{PPP}$ corresponding to the PPP transition sequences, with $\mathcal{P}^{(3)}_{PAP} + \mathcal{P}^{(3)}_{PPP} = \mathcal{P}^{(3)}$. To show that this is indeed the case we show in Fig. 8 the contour plot of the two-electron coincidence spectra associated with the highlighted area in Fig. 7 corresponding to the transitions $Ar^+(2p^{-1}) \rightarrow Ar^{2+}(2p^{-1}3s^{-1}) \rightarrow Ar^{3+}$. Note that the height of the peaks in Fig. 8 is given by $\mathcal{A}^{(3)}_{j\rightarrow k}$ or $\mathcal{A}^{(3)}_{j(i)\rightarrow k}$ (see discussion in section IIA) for the PPA transition sequences while the height is $\mathcal{P}^{(3)}_{j\rightarrow k}$ or $\mathcal{P}^{(3)}_{j(i)\rightarrow k}$ for the PPP and PAP transition sequences. Each coincidence peak has been convoluted by a 0.37 eV FWHM Gaussian function. We find that all except one of the observable peaks in Fig. 8 are due to PPA transition sequences; the small height peak at $(E_C = 211.7, E_B = 190)$ is due to a PAP sequence. We have thus demonstrated that we can retrieve from the two-electron coincidence spectra the Auger electron spectra associated with the transitions $Ar^{2+} \rightarrow Ar^{3+}$. We note that a similar discussion and conclusions hold for the Auger spectra corresponding to the $Ar^+(2p^{-1}_{1/2})$ fine structure state in Eq. (8).

Finally we note that our calculations neglect satellite structure. That is, we do not account for Auger transitions where one electron fills in the 2p hole, another one escapes to the continuum while a third one is promoted to an excited state. The main (larger) satellite Auger yields we are neglecting are most likely due to the $Ar^+(2p^{-1}) \rightarrow Ar^{2+}(3s^{-1}3p^{-1})$ transition[15]. However, these satellite yields are smaller than the main Auger yields for this transition. In addition, these satellite Auger yields would only contribute to the part of the spectrum corresponding to PAP transition sequences in the energy region E_B =170 -180 eV and E_C =210-220 eV. But as we discussed above the contribution to the electron spectra from PAP transition sequences is smaller than the contribution from the PPA transition sequences. Thus our approximation is justified.

IV. CONCLUSIONS

We have explored the interplay of photo-ionization and Auger transitions in Ar when interacting with a 260 eV FEL pulse. Solving the rate equations we have explored the dependence of the ion and Auger yields on the laser parameters accounting, at first, only for the electron configuration of the ion states. We have found that an FEL pulse of roughly 5 fs duration and 5×10^{15} Wcm^{-2} intensity is optimal for retrieving Auger electron spectra up to Ar^{3+}. Secondly, we have account for the fine structure of the ionic states and have truncated the rate equations to include states only up to Ar^{4+}. We have shown how the Auger electron spectra of $Ar^+ \rightarrow Ar^{2+}$ can be retrieved. We have also shown that the Auger electron spectra of $Ar^{2+} \rightarrow Ar^{3+}$ can also be retrieved when two electrons are considered in coincidence. We have thus demonstrated that interaction with FEL radiation is a possible route for retrieving Auger electron spectra. We believe that our work will stimulate further theoretical and experimental studies along these lines.

V. ACKNOWLEDGMENTS

The authors are grateful to Prof. P. Lambropoulos for initial motivation and valuable discussions. A.E. acknowledges support from EPSRC under Grant No. H0031771 and J0171831 and use of the Legion computational resources at UCL.

[1] A. A. Sorokin, S. V. Bobashev, T. Feigl, K. Tiedtke, H. Wabnitz, and M. Richter, Phys. Rev. Lett. **99**, 213002 (2007).

[2] L. Young, E. P. Kanter, B. Krässig, Y. Li, A. M. March, S. T. Pratt, R. Santra, S. H. Southworth, N. Rohringer, L. F. DiMauro, *et al.*, Nature **466**, 56 (2010).

[3] G. Doumy, C. Roedig, S. K. Son, C. Blaga, A. D. DiChiara, R. Santra, N. Berrah, C. Bostedt, J. D. Bozek, P. H. Bucksbaum, *et al.*, Phys. Rev. Lett. **106**, 83002 (2011).

[4] H. Fukuzawa, S.-K. Son, K. Motomura, S. Mondal, K. Nagaya, S. Wada, X.-J. Liu, R. Feifel, T. Tachibana, Y. Ito, *et al.*, Phys. Rev. Lett. **110**, 173005 (2013).

[5] L. J. Frasinski, V. Zhaunerchyk, M. Mucke, R. J. Squibb, M. Siano, J. H. D. Eland, P. Linusson, P. v. d. Meulen, P. Salén, R. D. Thomas, *et al.*, Phys. Rev. Lett. **111**, 073002 (2013).

[6] W. Mehlhorn, *Atomic Inner-Shell Physics* (Plenum, New York, 1985).

[7] E. J. McGuire, Phys. Rev. A **11**, 10 (1975).

[8] E. J. McGuire, Phys. Rev. A **11**, 1880 (1975).

[9] W. Mehlhorn and D. Stalherm, Z. Phys. **217**, 294 (1968).

[10] L. O. Werme, T. Bergmark, and K. Siegbahn, Phys. Scr. **8**, 149 (1973).

[11] F. Von Busch, J. Doppelfeld, C. Gunther, and E. Hartmann, J. Phys. B: At. Mol. Opt. Phys. **27**, 2151 (1994).

[12] U. Alkemper, J. Doppelfeld, and F. Von Busch, Phys. Rev. A **56**, 2741 (1997).

[13] F. von Busch, U. Kuetgens, J. Doppelfeld, and S. Fritzsche, Phys. Rev. A **59**, 2030 (1999).

[14] P. Lablanquie, S. M. Huttula, M. Huttula, L. Andric, J. Palaudoux, J. H. D. Eland, Y. Hikosaka, E. Shigemasa, K. Ito, and F. Penent, Phys. Chem. Chem. Phys. **13**, 18355 (2011).

[15] H. Pulkkinen, S. Aksela, O. P. Sairanen, A. Hiltunen, and H. Aksela, J. Phys. B: At. Mol. Opt. Phys. **29**, 3033 (1996).

[16] P. Lablanquie, L. Andric, J. Palaudoux, U. Becker, M. Braune, J. Viefhaus, J. H. D. Eland, and F. Penent, J. Elec. Spec. Rel. Phenom. **156**, 51 (2007).

[17] S. M. Huttula, P. Lablanquie, L. Andric, J. Palaudoux, M. Huttula, S. Sheinerman, E. Shigemasa, Y. Hikosaka, K. Ito, and F. Penent, Phys. Rev. Lett. **110**, 113002 (2013).

[18] N. Rohringer and R. Santra, Phys. Rev. A **76**, 033416 (2007).

[19] M. G. Makris, P. Lambropoulos, and A. Mihelič, Phys. Rev. Lett. **102**, 033002 (2009).

[20] C. P. Bhalla, N. O. Folland, and M. A. Hein, Phys. Rev. A **8**, 649 (1973).

[21] M. H. Chen and B. Crasemann, Phys. Rev. A **10**, 2232 (1974).

[22] H.-J. Werner, P. J. Knowles, G. Knizia, F. R. Manby, M. Schütz, *et al.*, "Molpro, version 2009.1, a package of ab initio programs," (2009), see http://www.molpro.net.

[23] F. Herman and S. Skillman, *Atomic structure calculations* (Prentice-Hall, New Jersey, 1963).

[24] M. D. Pauli, `http://hermes.phys.uwm.edu/projects/elecstruct/hermsk/HS.TOC.html`.

[25] B. Numerov, Publs. Observatoire Central Astrophys. Russ. **2**, 188 (1933).

[26] M. A. Melkanoff, T. Sawada, and J. Raynal, Methods Comp. Phys. **6**, 1 (1966).

[27] M. S. Child, *Molecular Collision Theory* (Academic Press, London, 1974).

[28] E. J. McGuire, Phys. Rev. A **3**, 1801 (1971).

[29] K. G. Dyall and F. P. Larkins, J. Phys. B: At. Mol. Phys. **15**, 2793 (1982).

[30] "Los Alamos National Laboratory Atomic Physics Codes," see `http://aphysics2.lanl.gov/tempweb/lanl/`.

[31] R. D. Cowan, *The theory of atomic structure and spectra* (University of California Press, 1981).

[32] W. H. Press, *Numerical Recipes: The art of scientific computing*, 3rd ed. (Cambridge University Press, 2007).

[33] P. Jönsson, G. Gaigalas, J. Bieroń, C. Froese Fischer, and I. P. Grant, Comput. Phys. Commun. **184**, 2197 (2013).

[34] S. Fritzsche, C. Froese Fischer, and G. Gaigalas, Comput. Phys. Commun. **148**, 103 (2002).

[35] S. Fritzsche, Comput. Phys. Commun. **183**, 1525 (2012).

[36] I. P. Grant, *Relativistic Quantum Theory of Atoms and Molecules: Theory and Computation (Springer Series on Atomic, Optical, and Plasma Physics)* (Springer-Verlag New York, Inc., 2006).

[37] M. Kurka, A. Rudenko, L. Foucar, K. U. Kühnel, Y. H. Jiang, T. Ergler, T. Havermeier, M. Smolarski, S. Schössler, K. Cole, *et al.*, J. Phys. B: At. Mol. Opt. Phys. **42**, 141002 (2009).

[38] A. Rudenko, Y. H. Jiang, M. Kurka, K. U. Kühnel, L. Foucar, O. Herrwerth, M. Lezius, M. F. Kling, C. D. Schröter, R. Moshammer, *et al.*, J. Phys. B: At. Mol. Opt. Phys. **43**, 194004 (2010).